Boundary conditions at the gas sectors of superhydrophobic grooves

Alexander L. Dubov,[1] Tatiana V. Nizkaya,[1] Evgeny S. Asmolov,[1,2] and Olga I. Vinogradova[1,3,4,*]

[1]*A.N. Frumkin Institute of Physical Chemistry and Electrochemistry, Russian Academy of Sciences, 31 Leninsky Prospect, 119071 Moscow, Russia*

[2]*Institute of Mechanics, M.V. Lomonosov Moscow State University, 119991 Moscow, Russia*

[3]*Department of Physics, M.V. Lomonosov Moscow State University, 119991 Moscow, Russia*

[4]*DWI Leibniz Institute for Interactive Materials, Forckenbeckstraße 50, 52056 Aachen, Germany*

(Received 26 July 2017; published 16 January 2018)

The hydrodynamics of liquid flowing past gas sectors of unidirectional superhydrophobic surfaces is revisited. Attention is focused on the local slip boundary condition at the liquid-gas interface, which is equivalent to the effect of a gas cavity on liquid flow. The system is characterized by a large viscosity contrast between liquid and gas $\mu/\mu_g \gg 1$. We interpret earlier results, namely, the dependence of the local slip length on the flow direction, in terms of a tensorial local slip boundary condition and relate the eigenvalues of the local local slip tensor to the texture parameters, such as the width of the groove δ and the local depth of the groove $e(y,\alpha)$. The latter varies in the direction y, orthogonal to the orientation of stripes, and depends on the bevel angle of the groove's edges, $\pi/2-\alpha$, at the point where three phases meet. Our theory demonstrates that when grooves are sufficiently deep their eigenvalues of the local slip length tensor depend only on μ/μ_g, δ, and α, but not on the depth. The eigenvalues of the local slip length of shallow grooves depend on μ/μ_g and $e(y,\alpha)$, although the contribution of the bevel angle is moderate. In order to assess the validity of our theory we propose an approach to solve the two-phase hydrodynamic problem, which significantly facilitates and accelerates calculations compared to conventional numerical schemes. The numerical results show that our simple analytical description obtained for limiting cases of deep and shallow grooves remains valid for various unidirectional textures.

DOI: 10.1103/PhysRevFluids.3.014002

I. INTRODUCTION

Anisotropic superhydrophobic (SH) surfaces have raised considerable interest in recent years. Such surfaces in the Cassie state, i.e., where the texture is filled with gas, can induce exceptional lubricating properties [1–3] and generate secondary flows transverse to the direction of the applied pressure gradient [4–6]. These are important for a variety of applications that involve a manipulation of liquids at the small scale and can be used to separate particles [7] and enhance their mixing rate [8,9] in microfluidic devices. Over the past decade the quantitative understanding of liquid flow past SH anisotropic surfaces has significantly expanded. However, many fundamental issues still remain unresolved.

To quantify the drag reduction and transverse hydrodynamic phenomena associated with SH surfaces with a given area of gas and solid fractions it is convenient to construct the effective slip boundary condition applied at the imaginary homogeneous surface [10,11], which mimics the real one and is generally a tensor [12]. Once eigenvalues of the local slip tensor, which depend on the local slip lengths at the solid and gas areas, are determined, they can be used to solve various hydrodynamic

*Corresponding author: oivinograd@yahoo.com

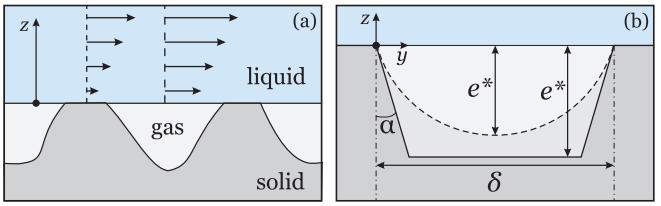

FIG. 1. (a) Sketch of the flow past a 1D superhydrophobic surface. (b) Sketch of trapezoidal (solid curve) and arc-shaped (dashed curve) grooves of width δ, maximal depth e^*, and bevel angle $\pi/2 - \alpha$.

problems. To calculate these eigenvalues, the SH surface is usually modeled as perfectly smooth with patterns of local boundary conditions at solid and gas sectors. It is widely accepted that one can safely impose no-slip boundary conditions at the solid area, i.e., neglect slippage of liquid past smooth solid hydrophobic areas, which is justified provided the nanometric slip is small compared to the parameters of the texture [13–16]. For gas sectors of SH surfaces the situation is much less clear. Prior work often applied shear-free boundary conditions at the flat gas areas [17–19]. In this idealized description both a meniscus curvature and a viscous dissipation in the gas phase, which could affect the local slippage, are fully neglected.

Several groups have recently studied the effect of a meniscus curvature on the friction properties of SH surfaces [20–24]. Most of these studies neglected a viscous dissipation in the gas by focusing on the connection of the meniscus protrusion angle and effective slip length (but note that no attempts have been made to connect the meniscus curvature and a local slip at the gas area). It has been generally concluded that if the protrusion angle is $\pm\pi/6$ or smaller, the effective slip of the SH surface does not differ significantly from what is expected in the case of the flat interface, so the model of a flat meniscus can always serve as a decent first-order approximation.

There is some literature describing attempts to provide a satisfactory theory of a local slip length, which take into account a viscous dissipation in the gas phase (and as far as we know, all these studies have modeled the liquid-gas interface as flat). We mention below what we believe are the most relevant contributions. To account for dissipation in gas it is necessary to solve the Stokes equations both for the liquid and for the gas phases [Fig. 1(a)], by imposing boundary conditions

$$\mathbf{u} = \mathbf{u}_g, \quad \mu \frac{\partial \mathbf{u}_\tau}{\partial z} = \mu_g \frac{\partial \mathbf{u}_{g\tau}}{\partial z} \quad \text{for} \quad z = 0, \tag{1}$$

where $\mathbf{u}$ and μ are the velocity and the dynamic viscosity of the liquid, respectively, $\mathbf{u}_g$ and μ_g are those of the gas, and $\mathbf{u}_\tau = (u_x, u_y)$ is the tangential velocity. This problem has been resolved numerically for rectangular grooves [25,26]. It is however advantageous to replace the two-phase approach with a single-phase problem with spatially dependent partial slip boundary conditions [1,27,28]. For unidirectional (1D) surfaces they are normally imposed as

$$\mathbf{u}_\tau - b(y) \frac{\partial \mathbf{u}_\tau}{\partial z} = 0 \quad \text{for} \quad z = 0, \tag{2}$$

where $b(y)$ is the local scalar slip length, which is varying in one direction only.

That the gas flow can be indeed excluded from the analysis being equivalently replaced by $b(y)$ is by no means obvious. Early work has suggested that the effect of gas-filled cavities is equivalent to the introduction of a slip length, proportional to their depth if shallow and to their spacing if deep [29]. To model the trapped gas effects theoretically a semianalytical method, which predicted a nonuniform local local slip distribution across the liquid-gas interface, was proposed [30,31]. In the past few years several authors have discussed that the local slip depends on the flow direction [31–33]. Although they did not fully recognize it, their results are equivalent to a tensorial generalization of

Eq. (2),

$$\mathbf{u}_\tau - \mathbf{b}\frac{\partial \mathbf{u}_\tau}{\partial z} = 0 \quad \text{for} \quad z = 0, \tag{3}$$

where $\mathbf{b}$ is the second-rank local local slip tensor, which is represented by a symmetric, positive-definite 2×2 matrix diagonalized by a rotation with respect to the alignment of the SH grooves.

Recent work has elucidated a mechanism which transplants the flow in the gas to a local slip boundary condition at the liquid-gas interface [33]. This study has concluded that the nonuniform local slip length of a shallow texture is defined by the viscosity contrast and local thickness of a gas cavity, similarly to infinite systems [34,35]. In contrast, the local slip length of a deep texture has been shown to be fully controlled by the dissipation at the edge of the groove, i.e., the point where three phases meet, but not by the texture depth, as has sometimes been invoked for explaining the extreme local slip. These results led to simple formulas describing liquid slippage at the trapped gas interface of 1D grooves of width δ and constant depth e^* [33],

$$b_{\parallel,\perp} \simeq \frac{\mu}{\mu_g}\delta\beta_{\parallel,\perp}, \tag{4}$$

where $b_{\parallel,\perp}$ are eigenvalues of the slip length tensor $\mathbf{b}$ and $\beta_{\parallel,\perp}$ are eigenvalues of the tensorial slip coefficient $\boldsymbol{\beta}$. The latter become linear in e^*/δ when e^*/δ is small and saturate at large e^*/δ. The validity of this ansatz for rectangular grooves has been confirmed numerically [33] and, although indirectly, experimentally [36].

Previous investigations have addressed the question of local slip at the gas areas of rectangular grooves with a constant depth only. We are unaware of any previous work that has quantified liquid slippage at gas areas of more general 1D SH surfaces. In this paper, we explore grooves with beveled edges and a nonuniform depth, which varies with y and depends on the bevel angle $\pi/2 - \alpha$ [see Fig. 1(b)]. An obvious practical advantage of such a relief is that the manufactured grooves become mechanically more stable against bending compared to rectangular ones. This is especially important for dilute textures of large δ, which induce larger slip. It is therefore very timely to understand important consequences of a bevel angle for a generation of liquid slippage at the gas areas of such grooves. Here we present theoretical arguments, which allow one to relate $b_{\parallel,\perp}$ to $e(y,\alpha)$. Our results show that $b_{\parallel,\perp}$ are not really sensitive to a bevel angle when SH grooves are shallow and weakly slipping, but the large local slip at deep SH grooves is controlled by their width and bevel angle only. These two parameters could be used to tune the large slip at the gas areas of any grooved SH surface and constrain its attainable upper value.

Our paper is organized as follows. In Sec. II we describe our model and justify the choice of model surfaces. Section III gives a brief summary of our theoretical results for $b_{\parallel,\perp}$ obtained in some limiting situations. In Sec. IV we describe a numerical method developed here to compute local local slip profiles. To solve numerically the two-phase hydrodynamic problem we consider separately flows in liquid and gas phases, which is in turn done by using different computational techniques. Our results are discussed in Sec. V and we summarize in Sec. VI. Details of our asymptotic analysis can be found in the Appendix.

II. MODEL

We consider creeping flow past 1D SH textures of period L and gas area fraction ϕ. The coordinate axis x is parallel to the grooves; the cross-plane coordinates are denoted by y and z. The width of the groove is denoted as $\delta = L\phi$. The bevel angle of the grooves is $\pi/2 - \alpha$, where an angle $\alpha \leqslant \pi/2$ is defined relative to the vertical, and the depth of the grooves $e(y,\alpha)$ is varying in only one direction [see Fig. 1(b)]. Since we consider SH textures with air trapped in the grooves in contact with water, the ratio of liquid and gas viscosities is typically $\mu/\mu_g \simeq 50$, which is much larger than unity. Our results apply to a situation where the capillary and Reynolds numbers are sufficiently small so that

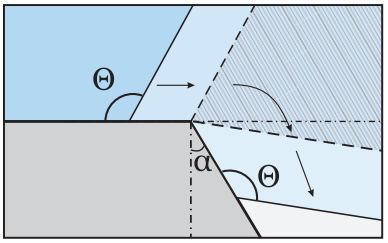

FIG. 2. Sketch of the contact angle, "measured" taking the horizontal as a reference, before, upon, and after the corner.

the liquid-gas interface does not deform, but not to the opposite case, where significant deformation of this interface is expected [37].

The texture material is characterized by the (unique) Young angle Θ (above $\pi/2$) measured taking the horizontal as a reference. Displacing a contact line to the sharp edge of a bevel angle $\pi/2-\alpha$, we would observe an apparent variability of the contact angle from Θ to $\pi/2-\alpha+\Theta$ since the line becomes pinned (see Fig. 2). Using simple geometry one can then conclude that in the Cassie state permitted protrusion angles of a meniscus are confined between $\pi/2+\alpha-\Theta$ and $\pi-\Theta$, so one of these (many) possible protrusion angles, which would be observed in practice, should be determined by a pressure drop between the liquid and the gas phases. Since positive protrusion angles (convex meniscus) are expected only when an external pressure is applied to the gas phase [23], we can exclude this artificial for SH surfaces case from our consideration. Now simple estimates suggest that for $\Theta=2\pi/3$, typical for SH texture materials, and when $\alpha=0$, bounds, which constrain attainable protrusion angles, are 0 (flat meniscus) and $-\pi/6$ (concave meniscus). Tighter bounds for finite α further constrain the attainable protrusion angle. These angles are too small to significantly reduce the effective slip [20,23]. Therefore, to highlight the effect of viscous dissipation on the slippage in simpler terms we here assume the liquid-gas interface to be flat, which implies that the pressure in the gas is equal to that in the liquid. Such a situation occurs when trapped by texture gas is in contact with the atmosphere [36].

Our aim is to investigate how the local depth $e(y,\alpha)/\delta$ modifies the slippage of liquid past gas areas. We will provide some general theoretical arguments and results valid for any shape of the SH grooves and also some simulation results for representative SH grooves. As an initial illustration of our theoretical and computational approach we will consider a trapezoidal surface, where α and the maximal depth e^* can be varied independently and in the very large range

$$e(y,\alpha)=\begin{cases} y\cot\alpha, & y\leqslant e^*\tan\alpha \\ e^*, & e^*\tan\alpha<y\leqslant\delta-e^*\tan\alpha \\ (\delta-y)\cot\alpha, & \delta-e^*\tan\alpha<y. \end{cases} \tag{5}$$

We mention that, motivated by a recent experiment [38], there have already been attempts to determine an effective slip past trapezoidal SH grooves [39], but that work simply assumed the trapezoidal shape of a local scalar slip and no attempt was made to properly connect it with viscous dissipation in the confined gas.

Grooves bounded by arcs of circles of radii $\delta/(2\cos\alpha)$ are another type of SH surface we explore here. These arc-shaped grooves do not have areas of a constant depth and the $e(y,\alpha)$ profile does not contain sectors where the dependence on α and δ disappears

$$e(y,\alpha)=\frac{\delta}{2}\left[\sqrt{\frac{1}{\cos^2\alpha}-\left(\frac{2y}{\delta}-1\right)^2}-\tan\alpha\right]. \tag{6}$$

Their maximal depth e^* is attained at the midplane $y/\delta = 0.5$ and is given by

$$e^* = \frac{\delta(1-\sin\alpha)}{2\cos\alpha}. \tag{7}$$

Equation (7) shows that arc-shaped grooves can never be really deep since e^*/δ cannot exceed 0.5. It will therefore be instructive to compare their local slip with that of trapezoidal textures of the same δ and e^*.

III. THEORY

Our aim is to calculate the eigenvalues of the local local slip tensor **b**, which can be found from the solution of the two-phase problem for the longitudinal (fastest) and transverse (slowest) flow directions by imposing conditions (1),

$$b_\parallel = \left.\frac{u_x}{\partial u_x/\partial z}\right|_{z=0} \equiv \frac{\mu}{\mu_g}\left.\frac{u_{g,x}}{\partial u_{g,x}/\partial z}\right|_{z=0}, \tag{8}$$

$$b_\perp = \left.\frac{u_y}{\partial u_y/\partial z}\right|_{z=0} \equiv \frac{\mu}{\mu_g}\left.\frac{u_{g,y}}{\partial u_{g,y}/\partial z}\right|_{z=0}. \tag{9}$$

However, since all properties of $\boldsymbol{\beta}$ are inherited by the local local slip tensor **b**, below we will focus more on calculations of scalar nonuniform eigenvalues $\beta_{\parallel,\perp}$.[1] In the general case they can be calculated only numerically. However, for some limiting cases explicit expressions can be obtained.

The solution for local slip lengths can be found analytically close to the edge of the grooves $y/\delta \ll 1$ and the details of our analysis are given in the Appendix. Here we highlight only the main results. Our theory predicts that in the vicinity of groove edges, the eigenvalues of local slip length of any 1D texture increase from zero as

$$b_\parallel \simeq \frac{\mu}{\mu_g}\frac{2y}{\tan(\pi/4+\alpha/2)}, \quad b_\perp \simeq \frac{b_\parallel}{4}. \tag{10}$$

It follows that at small y/δ the slip coefficient grows as

$$\beta_{\parallel,\perp} \simeq \beta'_{\parallel,\perp}\frac{y}{\delta} \tag{11}$$

by having slopes

$$\beta'_\parallel \simeq \frac{2}{\tan(\pi/4+\alpha/2)}, \quad \beta'_\perp \simeq \frac{1}{2\tan(\pi/4+\alpha/2)}. \tag{12}$$

Note that when $\alpha = 0$, Eqs. (12) predict $\beta'_\parallel \simeq 2$ and $\beta'_\perp \simeq 1/2$. If $\alpha = \pi/2$, i.e., there are no gas sectors, $\beta'_{\parallel,\perp} \simeq 0$. We also remark that the linearity of the Stokes equations implies that near the second edge of the groove $y/\delta = 1$, we have

$$\beta_{\parallel,\perp} \simeq \beta'_{\parallel,\perp}\left(1-\frac{y}{\delta}\right). \tag{13}$$

It has been suggested before that local slip length of a shallow groove is defined only by the viscosity contrast and local thickness of a thin lubricating films [32], similarly to infinite systems [34,35], but also depends strongly on the flow direction. Since in our case the local thickness depends on α, the early results [32] can be generalized as

$$b_\parallel \simeq \frac{\mu}{\mu_g}e(y,\alpha), \quad b_\perp \simeq \frac{b_\parallel}{4}, \tag{14}$$

[1] As a side note we mention that Eqs. (4), (8), and (9) suggest that $\delta\beta_{\parallel,\perp}$ can be interpreted as eigenvalues of the local slip lengths on the gas side of the interface.

and by using Eq. (4) we can immediately formulate equations for eigenvalues of a slip coefficient in this limit

$$\beta_{\parallel} \simeq e(y,\alpha)/\delta, \quad \beta_{\perp} \simeq \beta_{\parallel}/4. \tag{15}$$

Although Eqs. (11) and (13) are valid for any groove depth, in the case of weakly slipping shallow groves the contribution of dissipation in the area $y/\delta \ll 1$ should be small compared to the central part of the gas areas so that $\beta_{\parallel,\perp}$ are controlled by the groove depth as predicted by Eq. (15). However, for strongly slipping deep grooves $\beta_{\parallel,\perp}$ should depend mainly on α since their maximal values are constrained by $\beta'_{\parallel,\perp}/2$. This suggests that when grooves are deep, $\beta_{\parallel,\perp}$ are not sensitive to the shape of their bottom and should saturate at some $e(y,\alpha)/\delta$. Returning to Eq. (4), we conclude that the local slip length at the gas areas of sufficiently deep grooves is defined by the viscosity contrast, their width, and bevel angle, but not by their depth. This implies that δ and α are the only two parameters that could be used to tune the large local slip at SH surfaces. It is important to note that they also constrain its attainable upper value and we can conclude that for rectangular grooves $b_{\parallel}$ should be inevitably below $\mu\delta/\mu_g$ and that $b_{\perp}$ is always smaller than $\mu\delta/4\mu_g$. For grooves of the same δ with beveled edges these upper (and in fact unattainable) bounds will be even smaller.

IV. COMPUTATION OF THE TWO-PHASE FLOW NEAR SUPERHYDROPHOBIC GROOVES

A precise discussion of the flow in the vicinity of a SH surface requires a numerical solution of the self-consistent two-phase boundary problem, which is normally done by using finite element [40] or boundary element [41] methods. Here we suggest a simple alternative approach, which is easier to implement. We start by noting that Eq. (4) does not contain any parameters associated with the flow of liquid. This implies that if Eq. (4) is correct, then $\beta_{\parallel,\perp}$ are universal characteristics of the groove geometry only. However, applying the same $\beta_{\parallel,\perp}$ as boundary conditions yields different velocities at the gas-liquid interface, $u^{\rm int}_{x,y}(y) = u_{x,y}|_{z=0}$, since the solution of the Stokes equations in liquid depends on μ/μ_g and ϕ. This suggests that one can construct a simple iterative scheme to solve the two-phase problem. We apply a lattice-Boltzmann method (LBM) [42,43] to simulate gas flow. It is robust, easy to implement, and allows one to measure the velocity $\mathbf{u}_{g,\tau}$ and shear rate $\partial\mathbf{u}_{g,\tau}/\partial z$ at the interface independently.

We begin with a solution for $u^{\rm int}_{x,y}$ obtained for an isolated perfect slip stripe, i.e., in the limit of small ϕ [17],

$$u^{\rm int}_{x,y}\big/u^{\rm max}_{x,y} = \sqrt{1-(2y/\delta-1)^2}, \tag{16}$$

and impose it as a boundary condition to calculate a flow in the gas phase. The eigenvalues of the local slip coefficient can then be calculated using Eqs. (8) and (9). Note that it is also convenient to use a more accurate formula $u^{\rm int}_{x,y}/u^{\rm max}_{x,y} = \frac{\cosh^{-1}[\cos(\pi y)/\cos(\pi\phi/2)]}{\cosh^{-1}[1/\cos(\pi\phi/2)]}$, which is valid for an arbitrary ϕ [17,19], and that this velocity profile is very close to that given by Eq. (16) when $\phi \leqslant 0.5$.

These computed eigenvalues specify boundary conditions for liquid flow. We then solve the Stokes equations in liquid numerically by using a method based on Fourier series [32,44]. The solution satisfying these new partial slip conditions leads in turn to a better approximation for the velocity at the gas-liquid interface. At the next iteration we use this new velocity profile instead of Eq. (16) to compute more accurate values of $\partial\mathbf{u}_{g,\tau}/\partial z$ and $\beta_{\parallel,\perp}$, and so on, until an exact solution is obtained.

We use D3Q19 implementation of the LBM with the unit length set by the lattice step a, the time step Δt, and mass density $\rho_0 = 1$. The kinematic viscosity of the fluid is defined through the relaxation time scale τ as $\nu = (2\tau - 1)/6$ and kept constant in all the simulations at $\nu = 0.03$. The simulated system is built in such way that the upper boundary represents a liquid-gas interface [$z = 0$ in Fig. 1(b)] and the groove walls are perpendicular to the yz plane. For each simulation run the height of the system N_z is chosen equal to the maximal depth of the groove. To provide sufficient resolution of groove shapes we use a simulation domain of the size $N_y = \delta = 126a$, $N_x = 8a$, and $N_z = 12a - 122a$. To verify the results we have repeated separate runs with 2 times and 4 times

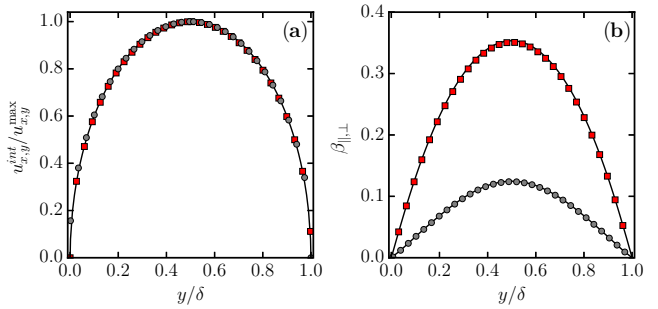

FIG. 3. (a) Dimensionless interface velocities $u^{\rm int}_{x,y}/u^{\rm max}_{x,y}$ and (b) eigenvalues of local slip coefficient $\beta_{\parallel,\perp}$ computed for a flow past trapezoidal grooves of $\alpha = 3\pi/32$ and $\phi = 0.5$. Symbols plot the results of the second iteration obtained for longitudinal (squares) and transverse (circles) grooves. Solid curves correspond to the first iteration step.

larger space resolution and have shown that the maximal error due to discretization does not exceed 1%. At the liquid-gas interface we set $\mathbf{u}_g|_{z=0} = (u^{\rm int}_x,0,0)$ for longitudinal and $\mathbf{u}_g|_{z=0} = (0,u^{\rm int}_y,0)$ for transverse grooves with $u^{\rm int}_{x,y}/u^{\rm max}_{x,y}$ given by Eq. (16). The maximum velocity $u^{\rm max}_{x,y}$ at $y = \delta/2$ is taken to be equal to $10^{-3}a/\Delta t$. At the gas-solid interface, given by $z = -e(y)$, where $e(y)$ is defined by Eq. (5) or (6), we impose no-slip boundary conditions. For trapezoidal grooves we have varied $N_z/N_y = e^*/\delta$ from 0.1 to 0.97 and α from 0 to $\pi/6$. For arc-shaped grooves the same values of α define $N_z = e^*$ [see Eq. (7)]. Finally, the periodic boundary conditions have been set along the x axis. All simulations are made with an open-source package ESPResSo [45].

To assess the validity and convergence of the approach we compute the interface velocity $u^{\rm int}_{x,y}/u^{\rm max}_{x,y}$ and the local slip coefficients $\beta_{\parallel,\perp}$ at fixed $\phi = 0.5$, $\alpha = 3\pi/32$, and $e^*/\delta = 0.97$. Figure 3 shows the interface velocity profiles and $\beta_{\parallel,\perp}$ obtained after two iteration steps. We conclude that both the longitudinal and transverse velocities at the gas sector nearly coincide with the predictions of Eq. (16) taken as an initial approximation, but we remark and stress that at the second iteration step $u^{\rm max}_{x,y}$ becomes quite different from that used as an initial guess. We also see that the $\beta_{\parallel,\perp}$ computed at the first and second iteration steps are practically the same. Therefore, in reality, our iteration procedure converges extremely fast, so below we use two iteration steps only.

Finally, to calculate the effective slip lengths for given computed local local slip profiles

$$b^{\parallel,\perp}_{\rm eff} = \left.\frac{\langle u_{x,y}\rangle}{\langle \partial_z u_{x,y}\rangle}\right|_{z=0} \tag{17}$$

we solve the Stokes equation in liquid numerically by using the Fourier series method described before in [32]. In these calculations we vary ϕ in the range from 0.1 to 0.9.

V. RESULTS AND DISCUSSION

We begin by studying the flow field in the gas phase of the grooves. For a longitudinal configuration the gas flows in the x direction only and its velocity monotonically decays from the gas-liquid interface to the bottom of the groove. The streamlines for a transverse case form a single eddy and the locus of its center depends slightly on the shape of the groove and on α. Figure 4 shows typical streamlines for a transverse flow in gas computed for trapezoidal grooves and arc-shaped grooves of $\alpha = 0$ and $\alpha = 3\pi/32$. The other parameters of a trapezoidal relief are taken to be the same as in Fig. 3. Note that with these parameters the trapezoidal grooves are roughly twice as deep as the arc-shaped grooves. Thus, if $\alpha = 0$, Eq. (7) gives $e^*/\delta = 1/2$ (cf. $e^*/\delta = 0.97$ for trapezoids). Altogether the simulation results show that the velocity field in the gas phase is not a unique function of α and that it generally depends on the relief of grooves and their depth. We note, however, that when the

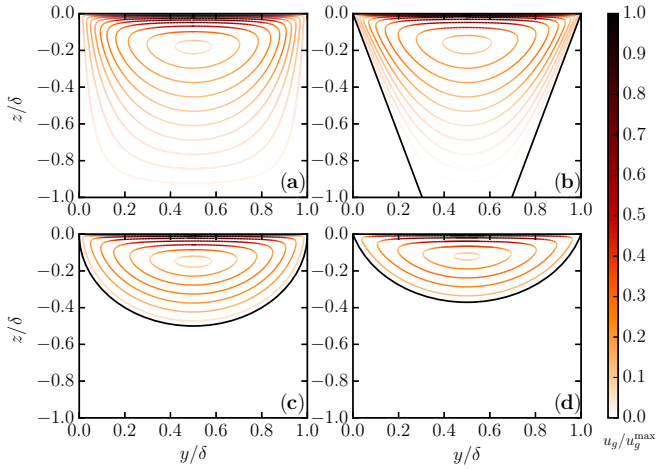

FIG. 4. Streamlines of the gas flow in the (a) and (b) trapezoidal and (c) and (d) arc-shaped transverse grooves of (a) and (c) $\alpha = 0$ and (b) and (d) $\alpha = 3\pi/32$. Color indicates the magnitude of velocity. Black lines show the gas-solid interface.

grooves are sufficiently deep, the gas in them is almost stagnant near the bottom, so increasing the depth further should not change the liquid flow past the SH surface.

The computed flow field in the gas phase allows one to immediately deduce $\beta_{\parallel,\perp}$. Figure 5 shows $\beta_{\parallel,\perp}$ for trapezoidal grooves of a fixed $\alpha = 3\pi/32$ and several depths e^*/δ. We see that for shallow grooves ($e^*/\delta \ll 1$) the $\beta_{\parallel,\perp}$ profiles can be approximated by trapezoids with the central region of a constant slip $\beta_\parallel \simeq e/\delta$ and $\beta_\perp \simeq e/4\delta$ given by Eqs. (15) and linear regions near edges with local slip coefficients described by Eqs. (11) and (13). For relatively deep grooves, $e^*/\delta = O(1)$, $\beta_{\parallel,\perp}$ profiles practically converge into single curves and are no longer dependent on e^*/δ. We also see that the crossover between the regimes of shallow and deep grooves takes place at intermediate e^*/δ, where $\beta_{\parallel,\perp}$ are controlled by both e^*/δ and α. To illustrate this we have included in Fig. 5 the $\beta_{\parallel,\perp}$ curves computed for arc-shaped grooves of the same $\alpha = 3\pi/32$, which implies that their $e^*/\delta \simeq 0.37$. Remarkably, the $\beta_{\parallel,\perp}$ profiles are very close to computed for trapezoidal grooves of $e^*/\delta = 0.35$. Some small discrepancies in the shapes of $\beta_{\parallel,\perp}$ obtained for two types of textures indicate that in the

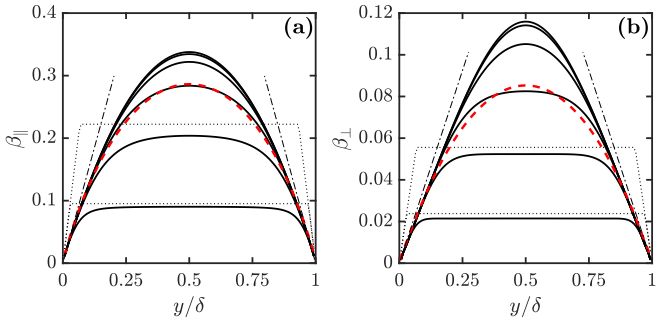

FIG. 5. (a) Longitudinal and (b) transverse slip coefficients for trapezoidal grooves computed at $\alpha = 3\pi/32$ (solid curves). From bottom to top $e^*/\delta = 0.094$, 0.22, 0.35, 0.47, 0.60, and 0.97. Dashed curves shows slip coefficient profiles for an arc-shaped groove with the same α and $e^*/\delta \simeq 0.37$. Dotted lines represent calculations with Eqs. (15) made with $e^*/\delta = 0.094$ and 0.22. Dash-dotted lines are predictions of Eqs. (11) and (13).

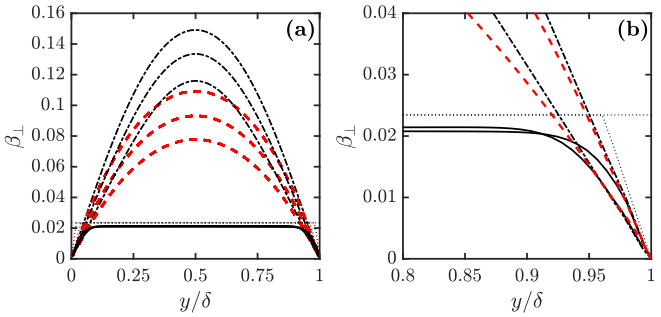

FIG. 6. (a) Transverse slip coefficient profiles for deep trapezoidal grooves of $e^*/\delta = 0.97$ (dash-dotted curves) and shallow trapezoidal grooves of $e^*/\delta = 0.094$ (solid curves). From top to bottom $\alpha = 0$, $\pi/16$, and $\pi/8$. The dotted line represents the prediction of Eq. (15) at $e^*/\delta = 0.094$. Dashed curves plot the results for arc-shaped grooves of the same values of α, which implies that e^*/δ is varying from 0.5 down to 0.32. (b) Data sets for $\alpha = 0$ reproduced in a larger scale in the vicinity of the edge $y/\delta = 1$ together with $\beta_\perp$ curves computed at $\alpha = 3\pi/32$.

crossover regime the shape of the grooves contributes to a local slip profile, but this should be seen as a second-order correction only.

Now we focus on the role of α and study first only deep, $e^*/\delta = 0.97$, and shallow, $e^*/\delta = 0.094$, trapezoidal grooves. The computed $\beta_\perp$ are displayed in Fig. 6(a). One can see that in the case of shallow textures $\beta_\perp$ generally does not depend on α and is consistent with Eq. (15), but note that there are deviations from Eq. (15) in the vicinity of the edges. For deep trapezoids it decreases with α. These trends agree fairly well with the predictions of Eqs. (11) and (12). We can now compare $\beta_\perp$ for deep trapezoidal grooves with that of arc-shaped grooves with the same bevel angle. The results of calculations are included in Fig. 6(a). The data show that at the central part of the gas sector the arc-shaped grooves induce smaller $\beta_\perp$ than trapezoidal ones, which simply reflects the fact that they are not deep enough. Indeed, with our values of α, their maximal depth e^*/δ varies from 0.5 down to 0.32, indicating the crossover regime. However, in the vicinity of the groove edges $\beta_\perp$ for both textures appears to be the same. To examine this more closely, the data obtained with two values of α in the edge region are plotted in Fig. 6(b) and we see that in the vicinity of the point where three phases meet the $\beta_\perp$ computed for different grooves indeed coincide. Altogether these results confirm that $\beta'_\perp$ is determined by α only.

Figure 7 includes $\beta'_{\parallel,\perp}$ curves computed for deep, $e^*/\delta = 0.97$, and shallow, $e^*/\delta = 0.094$, trapezoidal grooves and arc-shaped grooves. The calculations are made using several α in the range

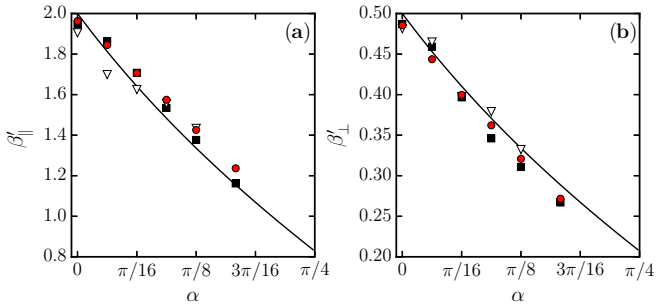

FIG. 7. Computed (a) $\beta'_\parallel$ and (b) $\beta'_\perp$ plotted as a function of α (symbols). Squares and triangles indicate trapezoidal grooves of $e^*/\delta = 0.97$ and 0.094 and circles plot the results for arc-shaped grooves. Calculations made with Eq. (12) are shown by solid curves.

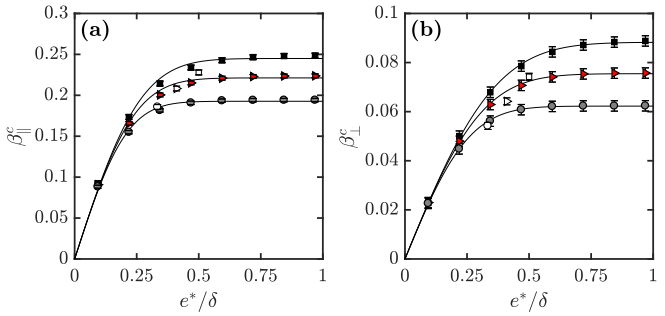

FIG. 8. Apparent slip coefficients $\beta^c_{\parallel,\perp}$ as a function of e^*/δ computed for trapezoidal grooves (closed symbols). From top to bottom $\alpha = 0$, $\pi/16$, and $\pi/8$. Error bars were determined from the deviation among repeated calculations made at different ϕ. When error bars are absent, uncertainties are smaller than the symbols. Solid curves are plotted to guide the eye. Open symbols correspond to $\beta^c_{\parallel,\perp}$ of arc-shaped grooves of the same α.

from 0 to $\pi/6$, which implies that e^*/δ varies from 0.5 down to 0.29. The general conclusion from this plot is that $\beta'_{\parallel,\perp}$ does not depend on the groove shape and depth being a function of α only, so our results fully verify Eq. (12).

We now turn to the effective slip lengths $b^{\parallel,\perp}_{\text{eff}}$ and will try to understand if such a two-phase problem can indeed be reduced to a one-phase problem and whether a SH surface can be modeled as a flat one with patterns of stripes with piecewise constant apparent local slip lengths $b^c_{\parallel,\perp}$. We first fit our numerical data for $b^{\parallel,\perp}_{\text{eff}}$ to the known formulas [28]

$$b^{\parallel}_{\text{eff}} \simeq \frac{L}{\pi}\frac{\ln\left[\sec\left(\frac{\pi\phi}{2}\right)\right]}{1+\frac{L}{\pi b^c_{\parallel}}\ln\left[\sec\left(\frac{\pi\phi}{2}\right)+\tan\left(\frac{\pi\phi}{2}\right)\right]},$$
$$b^{\perp}_{\text{eff}} \simeq \frac{L}{2\pi}\frac{\ln\left[\sec\left(\frac{\pi\phi}{2}\right)\right]}{1+\frac{L}{2\pi b^c_{\perp}}\ln\left[\sec\left(\frac{\pi\phi}{2}\right)+\tan\left(\frac{\pi\phi}{2}\right)\right]}, \tag{18}$$

taking $b^c_{\parallel,\perp}$ as fitting parameters, and then deduce $\beta^c_{\parallel,\perp}$, which can be defined as [33]

$$\beta^c_{\parallel,\perp} = \frac{\mu_g}{\mu}\frac{b^c_{\parallel,\perp}}{\delta}. \tag{19}$$

We stress that with such a definition the eigenvalues of apparent slip coefficients $\beta^c_{\parallel,\perp}$ of trapezoidal grooves depend only on α and e^*/δ, but not on y/δ. The curves for $\beta^c_{\parallel,\perp}$, computed for several α, are plotted in Fig. 8. For all α these functions saturate already at $e^*/\delta \geqslant 1$, thereby imposing constraints on the attainable $b^{\parallel,\perp}_{\text{eff}}$. Also included in Fig. 8 are $\beta^c_{\parallel,\perp}$ for arc-shaped texture of the same α. In this case $e(y,\alpha)/\delta$ is nonuniform throughout the cross section and we make no attempt to calculate its average or effective value at a given α. Instead, Fig. 8 is intended to indicate the range of $\beta^c_{\parallel,\perp}$, which is expected for arc-shaped grooves, so in this case we simply plot data as a function of e^*/δ. One can see that data for arc-shaped grooves nearly coincide with the results for trapezoidal grooves at $\alpha = \pi/8$, but at smaller angles there is some discrepancy, especially when $\alpha = 0$ and for a transverse case. The discrepancy is always in the direction of smaller $\beta^c_{\parallel,\perp}$ than found for trapezoidal grooves of $e = e^*$, indicating that the effects of the groove shape become discernible at intermediate depths. We stress, however, that for both trapezoidal and arc-shaped grooves the values of $\beta^c_{\parallel,\perp}$ are close and show the same trends. So our results for two types of grooves provide a good sense of the possible local slip of the 1D texture of any shape.

These results can be used to predict upper attainable local and effective slip lengths of complex grooves if their bevel angle and maximal depth are known. Indeed, Fig. 8 allows one to immediately

evaluate $\beta^c_{\parallel,\perp}$ and the apparent local slip lengths can be found by using Eq. (19). Once they are known, the eigenvalues of the effective length tensor can be calculated analytically by using Eqs. (18).

VI. CONCLUSION

We have analyzed liquid slippage at gas areas of 1D SH surfaces and developed an asymptotic theory, which led to explicit expressions for the longitudinal and transverse slip lengths near the edge of the groove, i.e., the point where three phases meet. The theory predicts that the local slip lengths in the vicinity of this point always increase linearly with the slope determined solely by a bevel angle of grooves. We have also shown that at a given viscosity contrast the eigenvalues of the local slip tensor of strongly slipping deep grooves are fully determined by their width and the value of their bevel angle, but not by their depth, as sometimes invoked for explaining the extreme local slip. Thus, it is not necessary to deal with very deep grooves to get a largest possible local slip at the gas areas. However, the eigenvalues of a local slip tensor of weakly slipping shallow grooves are not really sensitive to the bevel angle and are determined mostly by their depth.

Altogether, our study shows that for a given width, SH grooves with beveled edges are less efficient than rectangular ones for drag reduction purposes. However, the use of grooves with beveled edges appears as a good compromise between the positive effect of their stability against bending and a moderate reduction of the slippage effect due to a bevel angle. A very large local slip length can be induced by using wide grooves with beveled edges, which would often be impossible for wide rectangular grooves due to their bending instability.

To check the validity of our theory, we have proposed an approach to solve numerically the two-phase hydrodynamic problem by considering separately flows in liquid and gas phases, which can in turn be done by using different techniques. Our method significantly facilitates and accelerates calculations compared to classical two-phase numerical schemes. Generally, the numerical results have fully confirmed the theory for limiting cases. They have also clarified that at intermediate depths a particular shape of 1D SH surface modifies the local slip profiles, but only slightly.

Our strategy and computational approach can be extended to a situation of a sufficiently curved meniscus. Another fruitful direction could be to consider more complex 2D textures, which include various pillars and holes. Thus, they may guide the design of textured surfaces with superlubricating potential in microfluidic devices, tribology, and more. It would also be interesting to revisit recent analysis of an effective slip of SH surfaces and its various implications since our results suggest that instead of a piecewise constant slip length at the gas areas, a local tensorial slip should be employed to obtain more accurate eigenvalues of the effective local slip tensor. Finally, we mention that our approach can be immediately applied to compute local slip lengths of grooves filled by immiscible liquid of low or high viscosity.

ACKNOWLEDGMENT

This research was partly supported by the Russian Foundation for Basic Research (Grant No. 15-01-03069).

APPENDIX: LOCAL SLIP LENGTHS NEAR THE EDGE OF THE GROOVE

Here we obtain the solutions of the Stokes equations and explicit formulas for eigenvalues of the local slip length in the vicinity of the groove edge $(y,z) = (0,0)$. Following [39,46], we use polar coordinates (r,θ), so that $y/\delta = -r\cos\theta$ and $z/\delta = r\sin\theta$ (see Fig. 9), and focus on the case $r \ll 1$. We will show that in this situation the eigenvalues of the local slip length, $b_{\parallel,\perp}$ increasing linearly with r, are proportional to the viscosity ratio when it is large, $\mu/\mu_g \gg 1$, and decrease with α.

In the case of longitudinal grooves the velocity has only one component $\mathbf{u} = (u,0,0)$ and the Stokes equations reduce to the Laplace equation $\Delta u = 0$. The general solution implies a power-law

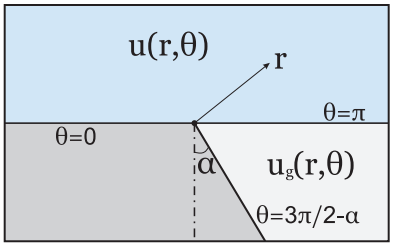

FIG. 9. Polar coordinates in the vicinity of the groove edge.

dependence of velocities on the distance

$$u_{l,g} = r^{\lambda_\parallel}[a_{l,g}\sin(\lambda_\parallel\theta) + c_{l,g}\cos(\lambda_\parallel\theta)], \tag{A1}$$

where an unknown exponent $\lambda_\parallel$ and coefficients a_l, a_g, c_l, and c_g can be found by imposing boundary conditions. These are defined in the usual way. Namely, we use the no-slip boundary conditions at the solid walls

$$u_l(r,0) = 0, \quad u_g(r,\theta_w) = 0, \tag{A2}$$

where $\theta_w = 3\pi/2 - \alpha$, and at the liquid-gas interface $\theta = \pi$ we impose

$$u_l = u_g, \quad \mu\partial_\theta u_l = \mu_g\partial_\theta u_g. \tag{A3}$$

Applying these boundary conditions, we obtain a linear homogeneous system

$$c_l = 0, \tag{A4}$$

$$a_g\sin(\lambda_\parallel\theta_w) + c_g\cos(\lambda_\parallel\theta_w) = 0, \tag{A5}$$

$$(a_l - a_g)\sin(\lambda_\parallel\pi) + (c_l - c_g)\cos(\lambda_\parallel\pi) = 0, \tag{A6}$$

$$(\mu a_l - \mu_g a_g)\cos(\lambda_\parallel\pi) - (\mu c_l - \mu_g c_g)\sin(\lambda_\parallel\pi) = 0, \tag{A7}$$

which allows us to derive an equation for $\lambda_\parallel$ by eliminating a_l, a_g, and c_g,

$$\tan\left[\lambda_\parallel\left(\frac{3\pi}{2} - \alpha\right)\right] = \frac{(\mu - \mu_g)\tan(\lambda_\parallel\pi)}{\mu + \mu_g\tan^2(\lambda_\parallel\pi)}. \tag{A8}$$

This result implies that the value of $\lambda_\parallel$ is determined by μ/μ_g and α. By expanding (A8) into a Taylor series in $\mu_g/\mu \ll 1$ we get

$$\lambda_\parallel = \frac{1}{2} - \frac{\mu_g}{\mu}\frac{\tan(\pi/4 + \alpha/2)}{\pi} + O\left(\frac{\mu_g^2}{\mu^2}\right). \tag{A9}$$

The longitudinal local slip profile near the edge of the groove can be then calculated as

$$b_\parallel = \frac{r\delta u_x(r,\pi)}{\partial_\theta u_x(r,\pi)} = -\frac{r\delta\tan(\lambda_\parallel\pi)}{\lambda_\parallel}. \tag{A10}$$

We note that the last equality has been obtained by using Eq. (A4). By using Eqs. (A9) and (A10) we can then derive, for $\mu/\mu_g \gg 1$,

$$b_\parallel \simeq \frac{\mu}{\mu_g}\frac{2y}{\tan(\pi/4 + \alpha/2)}. \tag{A11}$$

In the case of transverse grooves, the solution of the Stokes equations can be expressed in terms of a stream function ψ, which satisfies the biharmonic equation $\Delta^2\psi = 0$. A general solution in the liquid phase has the form [46]

$$\psi_l(r,\theta) = r^{\lambda_\perp}\{a_l \sin(\lambda_\perp\theta) + g_l \sin[(\lambda_\perp - 2)\theta] + c_l \cos(\lambda_\perp\theta) + h_l \cos[(\lambda_\perp - 2)\theta]\} \tag{A12}$$

and the radial and the angular components of the velocity are

$$u_{lr}(r,\theta) = \frac{\partial_\theta\psi}{r}, \quad u_{l\theta}(r,\theta) = -\partial_r\psi. \tag{A13}$$

The same equations are valid for a stream function ψ_g and velocities u_{gr} and $u_{g\theta}$, in the gas phase, with coefficients a_g, g_g, c_g, and h_g in Eq. (A12). To find the eight unknown coefficients and $\lambda_\perp$ we again apply the boundary conditions at the solid walls and at the liquid-gas interface. The no-slip conditions at the wall, $u_r = u_\theta = 0$ at $\theta = 0$ and $\theta = \theta_w$, allow us to formulate four equations of the system

$$c_l + h_l = 0, \tag{A14}$$

$$\lambda_\perp a_l + (\lambda_\perp - 2)g_l = 0, \tag{A15}$$

$$a_g \sin(\lambda_\perp\theta_w) + g_g \sin[(\lambda_\perp - 2)\theta_w] + c_g \cos(\lambda_\perp\theta_w) + h_g \cos[(\lambda_\perp - 2)\theta_w] = 0, \tag{A16}$$

$$\begin{aligned}&\lambda_\perp a_g \cos(\lambda_\perp\theta_w) + (\lambda_\perp - 2)g_g \cos[(\lambda_\perp - 2)\theta_w]\\ &-\lambda_\perp c_g \sin(\lambda_\perp\theta_w) - (\lambda_\perp - 2)h_g \sin[(\lambda_\perp - 2)\theta_w] = 0.\end{aligned} \tag{A17}$$

The conditions at the interface $\theta = \pi$, namely, of the impermeability $u_{l\theta} = u_{g\theta} = 0$ and of the continuity of the tangent velocity $u_{lr} = u_{gr}$ and the shear stress $\mu\partial_\theta u_{lr} = \mu_g\partial_\theta u_{gr}$, give

$$(a_l + g_l)\sin(\lambda_\perp\pi) + (c_l + h_l)\cos(\lambda_\perp\pi) = 0, \tag{A18}$$

$$(a_g + g_g)\sin(\lambda_\perp\pi) + (c_g + h_g)\cos(\lambda_\perp\pi) = 0, \tag{A19}$$

$$[(a_l - a_g)\lambda_\perp + (g_l - g_g)(\lambda_\perp - 2)]\cos(\lambda_\perp\pi) - [(c_l - c_g)\lambda_\perp + (h_l - h_g)(\lambda_\perp - 2)]\sin(\lambda_\perp\pi) = 0, \tag{A20}$$

$$\begin{aligned}&[(\mu a_l - \mu_g a_g)\lambda_\perp^2 + (\mu g_l - \mu_g g_g)(\lambda_\perp - 2)^2]\sin(\lambda_\perp\pi)\\ &+ [(\mu c_l - \mu_g c_g)\lambda_\perp^2 + (\mu h_l - \mu_g h_g)(\lambda_\perp - 2)^2]\cos(\lambda_\perp\pi) = 0.\end{aligned} \tag{A21}$$

The solution of the system of equations (A14)–(A21) cannot be reduced to a single equation for $\lambda_\perp$, as it has been done in the longitudinal case [and led to $\lambda_\parallel$ described by Eq. (A9)]. However, it is possible to obtain an asymptotic solution when $\mu/\mu_g \gg 1$,

$$\lambda_\perp = \frac{3}{2} - \frac{\mu_g}{\mu}\frac{2\tan(\pi/4 + \alpha/2)}{\pi} + O\left(\frac{\mu_g^2}{\mu^2}\right). \tag{A22}$$

The local transverse slip length can be calculated as

$$b_\perp = \frac{r\delta u_{lr}(r,\pi)}{\partial_\theta u_{lr}(r,\pi)} = \frac{r\delta\tan(\lambda_\perp\pi)}{2(\lambda_\perp - 1)}, \tag{A23}$$

where the last equality is obtained by using Eqs. (A14) and (A15). This immediately gives

$$b_\perp \simeq \frac{\mu}{\mu_g}\frac{y}{2\tan(\pi/4 + \alpha/2)} = \frac{b_\parallel}{4}. \tag{A24}$$

[1] L. Bocquet and J.-L. Barrat, Flow boundary conditions from nano- to micro-scales, Soft Matter **3**, 685 (2007).
[2] J. P. Rothstein, Slip on superhydrophobic surfaces, Annu. Rev. Fluid Mech. **42**, 89 (2010).
[3] O. I. Vinogradova and A. L. Dubov, Superhydrophobic textures for microfluidics, Mendeleev Commun. **22**, 229 (2012).
[4] F. Feuillebois, M. Z. Bazant, and O. I. Vinogradova, Transverse flow in thin superhydrophobic channels, Phys. Rev. E **82**, 055301(R) (2010).
[5] S. Schmieschek, A. V. Belyaev, J. Harting, and O. I. Vinogradova, Tensorial slip of super-hydrophobic channels, Phys. Rev. E **85**, 016324 (2012).
[6] J. Zhou, A. V. Belyaev, F. Schmid, and O. I. Vinogradova, Anisotropic flow in striped superhydrophobic channels, J. Chem. Phys. **136**, 194706 (2012).
[7] E. S. Asmolov, A. L. Dubov, T. V. Nizkaya, A. J. C. Kuehne, and O. I. Vinogradova, Principles of transverse flow fractionation of microparticles in superhydrophobic channels, Lab Chip **15**, 2835 (2015).
[8] J. Ou, G. R. Moss, and J. P. Rothstein, Enhanced mixing in laminar flows using ultrahydrophobic surfaces, Phys. Rev. E **76**, 016304 (2007).
[9] T. V. Nizkaya, E. S. Asmolov, and O. I. Vinogradova, Advective superdiffusion in superhydrophobic microchannels, Phys. Rev. E **96**, 033109 (2017).
[10] O. I. Vinogradova and A. V. Belyaev, Wetting, roughness and flow boundary conditions, J. Phys.: Condens. Matter **23**, 184104 (2011).
[11] K. Kamrin, M. Z. Bazant, and H. A. Stone, Effective slip boundary conditions for arbitrary periodic surfaces: The surface mobility tensor, J. Fluid Mech. **658**, 409 (2010).
[12] M. Z. Bazant and O. I. Vinogradova, Tensorial hydrodynamic slip, J. Fluid Mech. **613**, 125 (2008).
[13] L. Joly, C. Ybert, and L. Bocquet, Probing the Nanohydrodynamics at Liquid-Solid Interfaces Using Thermal Motion, Phys. Rev. Lett. **96**, 046101 (2006).
[14] O. I. Vinogradova and G. E. Yakubov, Dynamic effects on force measurements. 2. Lubrication and the atomic force microscope, Langmuir **19**, 1227 (2003).
[15] C. Cottin-Bizonne, B. Cross, A. Steinberger, and E. Charlaix, Boundary Slip on Smooth Hydrophobic Surfaces: Intrinsic Effects and Possible Artifacts, Phys. Rev. Lett. **94**, 056102 (2005).
[16] O. I. Vinogradova, K. Koynov, A. Best, and F. Feuillebois, Direct Measurements of Hydrophobic Slipage Using Double-Focus Fluorescence Cross-Correlation, Phys. Rev. Lett. **102**, 118302 (2009).
[17] J. R. Philip, Flows satisfying mixed no-slip and no-shear conditions, J. Appl. Math. Phys. **23**, 353 (1972).
[18] N. V. Priezjev, A. A. Darhuber, and S. M. Troian, Slip behavior in liquid films on surfaces of patterned wettability, Phys. Rev. E **71**, 041608 (2005).
[19] E. Lauga and H. A. Stone, Effective slip in pressure-driven Stokes flow, J. Fluid Mech. **489**, 55 (2003).
[20] A. M. J. Davis and E. Lauga, Geometric transition in friction for flow over a bubble mattress, Phys. Fluids **21**, 011701 (2009).
[21] M. Sbragaglia and A. Prosperetti, A note on the effective slip properties for microchannel flows with ultrahydrophobic surfaces, Phys. Fluids **19**, 043603 (2007).
[22] J. Hyväluoma and J. Harting, Slip Flow Over Structured Surfaces with Entrapped Microbubbles, Phys. Rev. Lett. **100**, 246001 (2008).
[23] E. Karatay, A. S. Haase, C. W. Visser, C. Sun, D. Lohse, P. A. Tsai, and R. G. H. Lammertink, Control of slippage with tunable bubble mattresses, Proc. Natl. Acad. Sci. USA **110**, 8422 (2013).
[24] D. G. Crowdy, Perturbation analysis of subphase gas and meniscus curvature effects for longitudinal flows over superhydrophobic surfaces, J. Fluid Mech. **822**, 307 (2017).
[25] D. Maynes, K. Jeffs, B. Woolford, and B. W. Webb, Laminar flow in a microchannel with hydrophobic surface patterned microribs oriented parallel to the flow direction, Phys. Fluids **19**, 093603 (2007).
[26] C. O. Ng, H. C. W. Chu, and C. Y. Wang, On the effects of liquid-gas interfacial shear on slip flow through a parallel-plate channel with superhydrophobic grooved walls, Phys. Fluids **22**, 102002 (2010).
[27] C. Cottin-Bizonne, C. Barentin, E. Charlaix, L. Bocquet, and J. L. Barrat, Dynamics of simple liquids at heterogeneous surfaces: Molecular-dynamics simulations and hydrodynamic description, Eur. Phys. J. E **15**, 427 (2004).

[28] A. V. Belyaev and O. I. Vinogradova, Effective slip in pressure-driven flow past super-hydrophobic stripes, J. Fluid Mech. **652**, 489 (2010).
[29] L. M. Hocking, A moving fluid interface on a rough surface, J. Fluid Mech. **76**, 801 (1976).
[30] C. Schönecker, T. Baier, and S. Hardt, Influence of the enclosed fluid on the flow over a microstructured surface in the Cassie state, J. Fluid Mech. **740**, 168 (2014).
[31] C. Schöenecker and S. Hardt, Longitudinal and transversal flow over a cavity containing a second immiscible fluid, J. Fluid Mech. **717**, 376 (2013).
[32] T. V. Nizkaya, E. S. Asmolov, and O. I. Vinogradova, Flow in channels with superhydrophobic trapezoidal textures, Soft Matter **9**, 11671 (2013).
[33] T. V. Nizkaya, E. S. Asmolov, and O. I. Vinogradova, Gas cushion model and hydrodynamic boundary conditions for superhydrophobic textures, Phys. Rev. E **90**, 043017 (2014).
[34] O. I. Vinogradova, Drainage of a thin liquid film confined between hydrophobic surfaces, Langmuir **11**, 2213 (1995).
[35] M. J. Miksis and S. H. Davis, Slip over rough and coated surfaces, J. Fluid Mech. **273**, 125 (1994).
[36] T. V. Nizkaya, A. L. Dubov, A. Mourran, and O. I. Vinogradova, Probing effective slippage on superhydrophobic stripes by atomic force microscopy, Soft Matter **12**, 6910 (2016).
[37] J. Seo, R. Garcia-Mayoral, and A. Mani, Pressure fluctuations and interfacial robustness in turbulent flows over superhydrophobic surfaces, J. Fluid Mech. **783**, 448 (2015).
[38] C. H. Choi, U. Ulmanella, J. Kimc, C. M. Ho, and C. J. Kim, Effective slip and friction reduction in nanograted superhydrophobic microchannels, Phys. Fluids **18**, 087105 (2006).
[39] J. Zhou, E. S. Asmolov, F. Schmid, and O. I. Vinogradova, Effective slippage on superhydrophobic trapezoidal grooves, J. Chem. Phys. **139**, 174708 (2013).
[40] V. Girault and P.-A. Raviart, *Finite Element Methods for Navier-Stokes Equations: Theory and Algorithms* (Springer Science + Business Media, Berlin, 2012), Vol. 5.
[41] C. Pozrikidis, *Boundary Integral and Singularity Methods for Linearized Viscous Flow* (Cambridge University Press, Cambridge, 1992).
[42] R. Benzi, S. Succi, and M. Vergassola, The lattice Boltzmann equation: Theory and applications, Phys. Rep. **222**, 145 (1992).
[43] L. S. Luo, Unified Theory of Lattice Boltzmann Models for Nonideal Gases, Phys. Rev. Lett. **81**, 1618 (1998).
[44] E. S. Asmolov, J. Zhou, F. Schmid, and O. I. Vinogradova, The effective slip-length tensor for a flow over weakly slipping stripes, Phys. Rev. E **88**, 023004 (2013).
[45] H. J. Limbach, A. Arnold, B. A. Mann, and C. Holm, ESPResSo—An extensible simulation package for research on soft matter systems, Comput. Phys. Commun. **174**, 704 (2006).
[46] C. Y. Wang, Flow over a surface with parallel grooves, Phys. Fluids **15**, 1114 (2003).